

1 **An Optical Coherence Tomography (OCT)-based Air Jet**  
2 **Indentation System for Measuring Mechanical Properties**  
3 **of Soft Tissues**

4 **Yan-Ping Huang**<sup>1</sup>, **Yong-Ping Zheng**<sup>1,2\*</sup>, **Shu-Zhe Wang**<sup>1</sup>, **Zhong-Ping Chen**<sup>3</sup>,  
5 **Qing-Hua Huang**<sup>1</sup>, and **Yong-Hong He**<sup>4</sup>

6 <sup>1</sup>Department of Health Technology and Informatics, <sup>2</sup>Research Institute of Innovative  
7 Products and Technologies, Hong Kong Polytechnic University, Hong Kong, China

8 <sup>3</sup>Beckman Laser Institute, University of California Irvine, Irvine, California, USA,

9 <sup>4</sup>Graduate School at Shenzhen, Tsinghua University, Shenzhen, China

10

11 **Running Title: OCT-based Air Jet Indentation**

12

13

14 Email: [ypzheng@ieee.org](mailto:ypzheng@ieee.org) and [hti.huang@polyu.edu.hk](mailto:hti.huang@polyu.edu.hk)

15

16 *Submitted to: Measurement Science and Technology*

17 First submission: May 27 2008; First revision: Aug 13 2008

18 **Abstract**

19 A novel noncontact indentation system with the combination of an air jet and optical  
20 coherence tomography (OCT) was presented in this paper for the quantitative  
21 measurement of mechanical properties of soft tissues. The key idea of this method is  
22 to use a pressure-controlled air jet as an indenter to compress the soft tissue in a non-  
23 contact way and utilize the OCT signals to extract the deformation induced. This  
24 indentation system provides measurement and mapping of tissue elasticity for small  
25 specimens with high scanning speed. Experiments were performed on 27 silicone  
26 tissue-mimicking phantoms with different Young's moduli, which were also measured  
27 by uniaxial compression tests. The regression coefficient of the indentation force to  
28 the indentation depth (N/mm) was used as an indicator of the stiffness of tissue under  
29 air jet indentation. Results showed that the stiffness coefficients measured by the  
30 current system well correlated with the corresponding Young's moduli obtained by  
31 conventional mechanical testing ( $r = 0.89$ ,  $p < 0.001$ ). Preliminary *in-vivo* tests also  
32 showed that the change of soft tissue stiffness with and without the contraction of the  
33 underlying muscles in the hand could be differentiated by the current measurement.  
34 This system may have broad applications in tissue assessment and characterization  
35 where alterations of mechanical properties are involved, in particular with the  
36 potential of noncontact micro-indentation for tissues.

37

38 **Keywords:** indentation, ultrasound indentation, soft tissue, elasticity,  
39 air-jet, optical coherence tomography

40 **1. INTRODUCTION**

41 In many tissue pathologies such as fibrosis, edema, and cancers in breast, liver and  
42 prostate, change of mechanical properties [1-4] is a common phenomenon observed by  
43 clinicians or patients themselves using the hand palpation. However, the hand palpation  
44 method is qualitative, at most semi-quantitative (such as the scoring system from the  
45 palpation impression), thus limiting its use in quantitative and objective studies. In the  
46 last two decades, in order to find optimal modalities for disease diagnosis and tissue  
47 assessment, more and more researchers are putting efforts in developing quantitative and  
48 objective approaches in the field of elasticity measurement and imaging based on  
49 ultrasound [5-15], MRI [16], or optical [17-22] measurements with the help of some kind  
50 of mechanical disturbances caused to the tissues including compression, indentation,  
51 suction, vibration, or acoustic radiation.

52 Indentation is currently one of the most frequently used techniques to measure the  
53 biomechanical properties of soft tissues [23-24]. Indentation, due to a small contact area  
54 with the tested objective, has the advantages of no necessity to excise the particular tissue,  
55 which is almost not possible for a standard uniaxial compression test, thus allowing its  
56 especial use for *in-vivo* applications. Traditional indentation system used a rigid indenter  
57 to compress the tissue in order to characterize the mechanical properties of soft tissue  
58 using the relationship between the force and deformation. However, usually no thickness  
59 information could be obtained directly from the indentation test. Tissue thickness is an  
60 important parameter for the diagnosis of some tissue pathologies such as cartilage  
61 degeneration [25] and is also an important factor for the calculation of tissue stiffness  
62 because this is included in the boundary condition of the theoretical analysis of the

63 indentation test [23]. The thickness was usually measured by extra post-test methods such  
64 as the needle probe penetration [26]. To address this issue, Zheng and Mak [7] had  
65 developed a portable ultrasound indentation system, which used the ultrasound transducer  
66 itself as an indenter. The system is capable of measuring both the initial thickness and  
67 stiffness. Due to its easy operation and a relatively compact profile fit for clinical  
68 operations, this ultrasound indentation system has been successfully applied in the  
69 assessment of a variety of tissues *in vivo*, including muscular tissues [27], residual limb  
70 tissues [28], diabetic foot plantar tissues [29], neck tissue fibrosis induced by  
71 radiotherapy [30-31], hypertrophic scar tissues [32-33], carpal tunnel ligament [34].  
72 Similar ultrasound indentation has also been used for the assessment of articular cartilage  
73 [35-36].

74 Typical ultrasound indentation uses an ultrasound transducer with the central  
75 frequency of 2~10 MHz for which the resolution is quite limited for small specimens  
76 such as the skin and articular cartilage. For transducers with a higher frequency the end is  
77 normally concave for better energy focus and larger penetration depth. In this case the  
78 transducer tip cannot be directly used as an indenter. Introduction of a bolster at the  
79 transducer tip for a planar indentation surface may possibly induce a poor coupling of the  
80 ultrasound signal and significantly attenuate the ultrasound signal, which severely affects  
81 the ultrasound measurement [36]. Furthermore, a rigid indenter is limited in achieving a  
82 fast scanning speed because of the requirement of point-wise measurement. To address  
83 these issues, a water jet indentation system had been developed [37-38]. In this system,  
84 the water jet serves as both the indenter and the coupling medium, thus significantly  
85 improving the speed in a C-scan test, i.e. the imaging plane is perpendicular to the

86 ultrasound beam [38]. Phantom tests showed that this system was capable of measuring  
87 the soft tissue elasticity quantitatively and reliably and also providing a fast C-scan  
88 mapping of the tissue elasticity. It has been further applied for the study of cartilage  
89 degeneration in a bovine patella model [39] and bone-tendon junction healing in a rabbit  
90 model [40] *in vitro*. The non-contact fluid indentation method also have the advantage of  
91 lowering the potential or risk of causing damage to the tested soft tissue, especially in  
92 tissues such as in scars or wounds where the contact indenter may cause inflammatory  
93 effects. Almost at the same time, another group reported a similar system using water jet  
94 for the assessment of articular cartilage [19]. They used an optical technique to detect the  
95 deformation applied by the water jet on the cartilage surface. Briefly, an optical beam  
96 with a constant intensity was illuminated onto the cartilage surface, and reflecting light  
97 was collected and its intensity was related to the local surface curvature, which was  
98 caused by the compression of the water jet.

99 One inconvenience to use the water-jet indentation is the water will split all over  
100 during the test. If it is used for tissues located inside body, the water or saline needs to be  
101 removed by another instrument. Another important factor for the widespread applications  
102 of prototype biomedical instrumentations to clinical situations is the potential of device  
103 miniaturization [41]. Even though miniaturization of ultrasound transducers is possible,  
104 such as those used for intra-vascular ultrasound imaging system, it is very expensive and  
105 the resolution is inherently limited. The water jet optical measurement system [19] used  
106 the intensity of the reflecting light to measure tissue deformation, but it is not accurate,  
107 particularly when the deformation is large or the tissue surface has different colours and  
108 textures.

109 In various optic methods, optical coherence Tomography (OCT) is a recent and fast  
110 developing technique that has acquired more and more widespread use in biomedical  
111 research [42]. The principle of OCT itself is analogous to that of the pulse-echo  
112 ultrasound imaging. It collected backscattered signals from the optically scattering tissues  
113 for the purpose of a cross-sectional imaging. The difference with respect to ultrasound is  
114 that OCT uses the optical interferometric rather than absolute time of flight technique to  
115 resolve the spatial information. Using an optical interferometric method, OCT has the  
116 high resolution thanks to the small coherence length of the light sources. Axial and lateral  
117 resolutions in a range of several microns can be achieved, thus making the optical biopsy  
118 a unique and attractive characteristic of this technique [43-45]. Similar to the ultrasound  
119 signals, the OCT can measure the thickness of tissue layers where normally at the  
120 interfaces the refractive index is abruptly changed. For example, one of the most  
121 important applications of OCT is pachymetry, i.e., to measure the corneal thickness *in*  
122 *vivo* for the use of diagnosis or surgery guide [46-47]. OCT-based elasticity imaging for  
123 tissues has also been widely investigated using contact compression [18,20-21]. In  
124 comparison with ultrasound elastography, OCT-based technique can provide higher  
125 resolutions. However, these elasticity imaging techniques can normally provide contrast  
126 of local strains but not an absolute value of tissue elasticity.

127 The integration of an OCT probe with the air jet indentation was realized in the  
128 current study to develop a novel system to measure the mechanical properties of soft  
129 tissues. The construction of the system was first described in the next section, then  
130 experimental and data analysis methods on phantoms and *in vivo* hand soft tissues, and  
131 the corresponding results were presented to demonstrate the utility of the current system,

132 and finally further issues related to the limitations, further improvement and applications  
133 of the current system in biomedical engineering were discussed before the study was  
134 concluded.

135

## 136 **2. METHODS**

### 137 *2.1. System Setup*

138 The schematic of the OCT-based air jet indentation system including the core part  
139 and the data collection part is shown in Figure 1 and Figure 2, respectively. The fiber-  
140 based OCT probe was modified to allow the installation of an air jet bubbler. The OCT  
141 system (Developed by Lab of Optical Imaging and Sensing, Graduate School at  
142 Shenzhen, Tsinghua University, China) has a super luminescent diode (SLD) light source  
143 (DenseLight, DL-CS3055A, Singapore) with a central wavelength of 1310 nm, a nominal  
144 -3 dB spectral bandwidth of 50 nm and a nominal output power of 5 mW. The axial  
145 resolution is 18  $\mu\text{m}$  and the imaging depth is approximately 2~3 mm in turbid high  
146 scattering tissues. The OCT probe was fixed in this study and the laser beam focuses  
147 vertically at around 5 mm under the lower surface of the bubbler. For convenience of the  
148 detection, a visible red light beam was used with the invisible infrared beam to guide the  
149 detection point. A pipeline with maximally constant air pressure was connected to the  
150 system to provide the air jet for the indentation. To make the air jet more uniform, a tube  
151 with an orifice diameter of 2 mm and a length of 5 mm was installed at the tip of bubbler  
152 to guide the air jet before it was pushed into free space. A calibrated pressure sensor  
153 (PMP 1400, GE Druck, Leicester, England) with a measurement range of 1 bar ( $10^5$  Pa)  
154 was installed before the bubbler to measure the pressure in the air pipe. A mechanical

155 valve was installed before the pressure sensor to adjust the pressure of the air jet  
156 continuously. A transparent plate was installed at the top of the bubbler to seal the  
157 pressurized air from the OCT components but let the laser beam to pass through.

158 A PC was used to control the operation of the system. A data acquisition card (DAQ,  
159 PCI-6251, National Instruments, Austin, TX, USA) was used through  
160 intercommunication to both control the main unit of OCT and collect the optical signals.  
161 Another DAQ card (PCI-6024E, National Instruments, Austin, TX, USA) was used to  
162 collect the signal from the pressure sensor. A custom-written program was developed in  
163 Microsoft VC++ for the signal synchronization and data collection (Figure 3). During the  
164 indentation process, the signals from the OCT and the pressure sensor were synchronized,  
165 sampled, displayed in real-time and saved for off-line processing by the program. In this  
166 study, the OCT scanning was continuously performed at a single location to track the  
167 surface displacement, which was assumed to be equivalent to the deformation of the  
168 tested specimen. The digitized A-scan signal was acquired at a rate of approximately 3.1  
169 Hz and the pressure signal was also sampled at this rate in synchronization with the A-  
170 scan signal. Each A-scan signal contained 7500 points of effective digital data for  
171 analysis. By using the two surfaces of a glass slide with a standard thickness for distance  
172 calibration, we obtained an equivalence of  $0.43 \mu\text{m}$ /per point for each A-line of the signal  
173 in air after calibration considering the difference of the refractive indices in glass and air.  
174 The displacement of the surface was extracted by applying a cross-correlation algorithm  
175 to the A-line signals, which was used to seek the most similar part to a pre-selected  
176 region of interest (ROI) in the A-scan signals recorded during the indentation process.  
177 The air-specimen interface was used as the pre-selected ROI in this study. In order to

178 reduce the effect of signal phase change during indentation and assure a better tracking,  
179 amplitude signal obtained by applying a Hilbert transform to the original optical signal  
180 was employed for the tracking. The same software using a different control panel was  
181 used to conduct the algorithms of cross-correlation for the extraction of the deformation  
182 (Figure 3).

## 183 2.2. *Phantoms and In-Vivo Tests*

184 We tested the system on 27 uniform tissue-mimicking silicone phantoms with  
185 different stiffness. They were made of three kinds of silicone materials with low viscosity:  
186 Rhodia RTV 573 (Rhodia Inc., CN7500, Cranbury, NJ, USA), Wacker M4648 and  
187 M4640 (Wacker Chemicals Hong Kong Ltd., HK, China). For each type of silicone, there  
188 were two parts A & B before mixing to make the phantom. Different proportions of A &  
189 B were mixed to make phantoms with different stiffness. Here we chose three different  
190 silicone materials to make phantoms covering a wide range of stiffness because phantom  
191 stiffness was not only dependent on the mixing ratio of the two parts but also on the  
192 silicone type. Three categories of phantom dimensions with a surface area of  $10 \times 10$   
193  $\text{mm}^2$  and a thickness of 5, 10 and 15 mm were fabricated [37]. All the experiments were  
194 conducted on the  $10 \times 10 \text{ mm}^2$  surface but with different phantom initial thickness (5, 10  
195 or 15 mm). During the air jet indentation, the phantom was fixed at edges by four screws  
196 and the air jet was exerted at the center of the surface. For each phantom, the axial  
197 distance of the phantom surface to the bubbler bottom was adjusted to be approximately 5  
198 mm based on the optical signal detected from the surface. If the specimen was too close  
199 to the bubbler, it would be attracted toward the bubbler by a force induced by the high  
200 velocity of the scattered air jet and the low pressure incurred around. Before each

201 indentation, the phantom was compressed and relaxed for several times to obtain a rigid  
202 fixation on the platform. Then the air jet indentation was exerted at a pressure changing  
203 rate of approximately 10 kPa/s and between 0 and 100 kPa, which corresponded to a  
204 maximum displacement of about 0.37 mm for the softest phantom. The maximum  
205 indentation depth was less than 5% for the phantom test. A typical test, including 1 to 2  
206 cycles of indentation, was finished in approximately 30 s. For the purpose of comparison,  
207 indentation tests with a rigid steel indenter (called standard indentation) and standard  
208 compression tests were also performed using a standard mechanical testing machine  
209 (Instron 5569, Norwood, MA, USA). For these two mechanical tests, the maximum  
210 indentation or compression depth was about 10% of the initial thickness (only the data  
211 within 3% deformation were used for parameter calculation) and the indentation speed  
212 was controlled to be 4 mm/min, which was similar to that of the air jet indentation.

213 In order to demonstrate the biomechanical applications of the system, a preliminary  
214 test was performed on soft tissues of the hand *in vivo* to differentiate the contraction state  
215 of the underlying muscle layer involved. Ten subjects (7 males, 3 females) without any  
216 lesions in the hand and with a mean age of  $27.8 \pm 2.9$  years (minimum: 23; maximum 32)  
217 were recruited in this test. A test site near the basal joint of the dorsal hand including the  
218 muscles of the first interosseous was selected for experiment (Figure 4). The subjects  
219 were asked to be seated in a natural posture with their hand placed on the platform. Two  
220 states of the muscle, i.e. relaxation and contraction, were produced by natural extension  
221 and forced adduction of the thumb (Figure 4). A deformation of approximately 1.5 mm  
222 was applied on the tissues using the air jet. The corresponding indentation deformation  
223 and forces were then collected and used for the calculation of the stiffness parameter.

224 **2.3. Data Analysis Method**

225 In the current study, the air jet indentation was assumed to be similar to the  
226 indentation with a rigid contact, by hypothesizing that the air pressure measured in the  
227 pipe was linearly proportional to the force induced on the specimen. The proportionality  
228 of the fluid pressure and the indentation force was earlier validated for the water jet case  
229 [37]. For the phantom tests, a stiffness coefficient  $k_{aj}$  (N/mm) regarding the regression  
230 ratio of the air jet indentation force (N) and deformation (mm) of the tested specimen was  
231 used to represent the stiffness of the phantom. This parameter was used here because with  
232 the assumption of a linear elasticity, a constant Poisson's ratio and a small aspect ratio  
233 (indenter radius/initial thickness  $a/h$ , in this study it was all less than 0.2), the  
234 indentation formula was [23]:

235 
$$E = (1 - \nu^2) / (2a\kappa(\nu, a/h)) \cdot F/d \quad (1)$$

236 where  $E$  the Young's modulus of the tissue,  $a$  the radius of the indenter,  $h$  the initial  
237 thickness of the tissue,  $\nu$  the Poisson's ratio of the tissue,  $\kappa$  a scaling factor related to  $\nu$   
238 and  $a/h$ ,  $F$  the indentation force and  $d$  the indentation depth. For the elastic material,  
239 Equation 1 is simplified to:

240 
$$E = (1 - \nu^2) / (2a) \cdot F/d \quad (2)$$

241 with  $\kappa$  approaching to one in Equation 1 [23,29,48]. The indentation force was  
242 computed by multiplying the measured air pressure with the area of the bubbler orifice  
243 ( $\phi = 2a = 2 \text{ mm}$ ). The corresponding stiffness coefficient obtained by the standard  
244 indentation was indicated by  $k_{std}$ . For the standard compression test, the Young's  
245 modulus ( $E$ ) of phantom could be obtained after computing the corresponding stress and  
246 strain. We assumed a homogeneity of the compressive properties of the phantom so one

247 value of Young's modulus would represent all at each specific point. The deformation  
248 ratio (deformation/initial thickness) or strain was constrained to be within 3% in all the  
249 calculation in order to obtain a coefficient within the linear elasticity region of  
250 compression of the phantoms [49]. Due to a low viscosity of the silicone phantoms, data  
251 of both the loading and unloading processes were utilized for the calculation of the  
252 stiffness coefficient. Pearson correlation coefficient was used to indicate the relationship  
253 among the measured parameters from the air jet indentation, the standard indentation and  
254 compression test.

255 For the *in-vivo* test, a corresponding stiffness coefficient  $k$  (N/mm) regarding the  
256 force/deformation ratio was calculated from the test and the average value of three  
257 repeated tests was used for each muscle contraction state. It should also be noted the  
258 mechanical properties measured from the hand soft tissue were characteristic of the  
259 whole tissue layer which might include the layers of skin, fat and muscles, but not that of  
260 a separate single layer. When the whole tissue layer undergoes some pathological or  
261 physiological changes such as the muscle contraction in the current study, the whole  
262 tissue will behave differently. Therefore, the measurement of overall tissue properties is  
263 also meaningful for the detection of tissue state under these conditions. A paired  $t$ -test  
264 was used to compare the change of the stiffness coefficient  $k$  for the soft tissues with and  
265 without muscle contraction. All the statistical analyses were performed in SPSS 14.0  
266 (SPSS, Chicago, IL, USA). In all the statistical tests,  $p < 0.05$  was used to indicate a  
267 significant correlation or a significant difference of the mean between two measures.

268

269 **3. RESULTS**

270 The results of a representative indentation test on the phantom are shown in Figure 5.  
271 Using the cross-correlation algorithm, the displacement could be successfully extracted  
272 out during the indentation in the phantom tests. Some noise with the extracted  
273 deformation was found during the processing, for which the reason was discussed in  
274 detail in the next section. A high correlation coefficient, normally larger than 0.95, was  
275 observed for the indentation force and deformation. A reliability test of 10 times of  
276 repeated experiments on one phantom showed that  $k_{aj}$  was  $1.108 \pm 0.035$  N/mm (3.2%  
277 for the coefficient of variation), which showed the test was highly reliable. Correlation  
278 tests among  $k_{aj}$ ,  $k_{std}$  and  $E$  are shown in Figure 6. A high correlation of  $r = 0.88$   
279 ( $p < 0.001$ ) was found for  $k_{aj}$  and  $k_{std}$ , which showed that the results of the two tests  
280 were highly comparable. A larger value of  $k_{aj}$  was consistently observed from the air jet  
281 indentation system than  $k_{std}$ , which might be attributed to the fact that a larger pressure  
282 was measured inside the air pipe than at the surface of the specimen where the air jet  
283 induced the deformation. The compression test showed that the stiffness of the phantoms  
284 was  $558 \pm 124$  kPa with a range of  $328 \sim 818$  kPa. A comparison between  $k_{aj}$  and  $E$   
285 also showed a high correlation ( $r = 0.89$ ,  $p < 0.001$ ), which indicated the current system  
286 could be used as a new approach to measure the mechanical properties of soft tissues.

287 *In-vivo* test showed that the stiffness coefficient was  $0.059 \pm 0.031$  N/mm and  $0.150$   
288  $\pm 0.059$  N/mm with the muscle in the relaxation and contraction states, respectively. A  
289 paired *t*-test showed that the soft tissue was significantly stiffer in the state of muscle

290 contraction ( $p < 0.001$ ). Therefore, the current system was capable of differentiating the  
291 state of the muscle contraction.

292

#### 293 **4. DISCUSSION**

294 An air jet indentation system utilizing the optical signals from the OCT system was  
295 developed and tested to demonstrate its capability in measuring the mechanical properties  
296 of soft tissues. Preliminary results on silicone phantoms and *in vivo* soft tissues of the  
297 hand showed that it was feasible to use the air jet indentation system to quantitatively  
298 measure the stiffness and further to detect the change of stiffness that might be involved  
299 in various tissue pathologies. The air jet was thought to be very convenient for use,  
300 because no extra mechanism was needed to collect the splitting medium, as in the water  
301 jet case. The incorporation of the OCT signal enabled the detection of deformation  
302 (displacement) as small as less than 1  $\mu\text{m}$ , and provided the potential for miniaturization  
303 for use in applications such as endoscopy. Compared to the rigid contact indentation  
304 method, this novel air jet indentation system also provided a potential for testing in fine  
305 tissues and a fast scanning to map the deformation distribution in soft tissues.

306 In the current study, OCT signals were introduced to extract the deformation of the  
307 indented specimen. The deformation was obtained by assuming that the platform  
308 underlying the specimen was fixed and then it was equivalent to track the surface  
309 movement. In real situations, the deformation as well as the thickness of the tissue can be  
310 measured directly from the OCT signal, provided that the whole tissue layer can be  
311 penetrated by the optical beam. This is also the advantage of using OCT for the air-jet  
312 measurement system in comparison with other optical methods for surface displacement

313 measurement. In the current study, the measured stiffness coefficient represents the  
314 mechanical properties of the whole tissue layer. During the data processing, it was found  
315 that the optical signals were quite sensitive to the movement of the surface of the  
316 specimen, even in the phantom test where the phantoms were firmly fixed. This might be  
317 caused by the surface roughness of the skin and the orientation change of the optical  
318 beam with non-vertical incidence during indentation. This sensitivity had brought some  
319 noise to the deformation in tracking. When necessary, the moving average was used in  
320 the current study to reduce the effect of noise. The movement sensitivity was one of the  
321 big differences noted by us between the OCT and ultrasound signals. We had not  
322 encountered such a problem previously in processing the ultrasound signal. This might be  
323 due to the uncertain change of the phases in the OCT signals with respect to the surface  
324 signal. This sensitivity might induce some tracking challenges in experiments,  
325 particularly tests on tissues *in vivo*, where the tissue self-motion during indentation is  
326 inevitable such as that caused by the respiration and heartbeat. Therefore in the current  
327 design of soft tissue test *in vivo*, a roughly constant indentation depth was produced by  
328 the air jet and then we measured the corresponding force in order to calculate the stiffness  
329 coefficient. Another issue for using the cross-correlation algorithm was the decorrelation  
330 caused by a large displacement. However, we thought the effect of decorrelation might  
331 not be so significant in the current study due to two main reasons: one was that the  
332 envelop signal was obtained to exclude or reduce the effect of phase change in tracking;  
333 the other was that we only detected the abrupt change of the surface signal, which was  
334 relatively easier to be tracked by choosing the ascending part of the signal at the surface.  
335 The sensitivity of signal shape and signal to noise ratio to the movement tracking of the

336 specimen surface and approaches for lowering this sensitivity for a more reliable tracking  
337 need to be further investigated.

338 The axial resolution of the OCT system used in this study was 18  $\mu\text{m}$ , which was the  
339 limit for the system to differentiate signals generated by two neighboring interfaces.  
340 Since in the current study we were interested in the movement of a distinguished  
341 interface, i.e. phantom surface or skin surface, we were able to achieve a much higher  
342 displacement resolution beyond the axial resolution, given that the decorrelation of the  
343 signal was small. The displacement resolution for the distinguished surface was mainly  
344 determined by the number of data points for a certain period of OCT signal, which  
345 represented a certain distance in the medium. In this study, we collected 7500 data points  
346 for a distance of approximately 3.22 mm (this value depends on the refractive index of  
347 the medium). Therefore, the displacement resolution of the interface movement was  
348 approximately 0.43  $\mu\text{m}$ . Such a displacement resolution for interface tracking can be  
349 achieved even when the OCT signals generated by two neighboring interfaces was  
350 overlapped, i.e. the distance between the two interfaces is smaller than the axial  
351 resolution of the measurement system, given that the two interfaces have no relative  
352 motion during the movement. However, the displacement resolution discussed above can  
353 not be applied to the movements of interfaces with the distance smaller than the axial  
354 resolution and involving relative motions, as this will cause decorrelation to the OCT  
355 signals. Under this condition, we are not able to tell which interface contributes to the  
356 displacement of the signal and the displacement resolution will be significantly reduced.  
357 The above discussion can not only be applied to the movement of the surface interfaces  
358 but also those inside the media. Apparently, the displacement resolution of 0.43 $\mu\text{m}$  for

359 the interface movement cannot be applied to the movement of scatters inside the medium,  
360 as the distances among scatters are very small and a smaller relative motion among them  
361 will cause large decorrelation to the signal. That is why the displacement resolution for  
362 ultrasound elastography [5], which aims to map tissue displacement or strain but not to  
363 measure the displacement of a certain interface, is normally limited by the axial  
364 resolution of the imaging system. In addition to signal decorrelation, cross-correlation  
365 tracking for signals can also be affected by the signal to noise ratio and the sampling rate  
366 of the signals. To measure tissue motion more accurately, it is worthwhile to  
367 systematically investigate the displacement resolution of the proposed OCT air jet system  
368 for the tissue interface and scatters inside the tissue in future studies.

369 A single point of displacement was measured in the current study using the A-line  
370 OCT signal to obtain the deformation of the whole specimen layer. In further studies,  
371 cross-sectional scanning, as used in B-mode ultrasound imaging, can be used to further  
372 study the problem such as the deformation profile under the air jet, as long as the lateral  
373 scanning can cover the size of the bubbler orifice. The frame rate of OCT A-line used in  
374 this study was relatively low. Though it did not affect the measurement for the phantoms  
375 and the carefully selected region of the hand, it should be significantly improved when a  
376 cross-sectional scanning is required. Utilizing the cross-sectional imaging, the  
377 elastography, which has been studied extensively in ultrasound and MR imaging field  
378 [5,16], can also be performed, provided the air jet induces the required deformation to the  
379 specimen [18]. One of the advantages of OCT compared to ultrasound is that the OCT is  
380 easier for minimization due to the fast development of optical technologies and devices.  
381 OCT probes for the endoscopic use in human mucosa had already been reported in the

382 literature [50-51]. Therefore, another aspect of further development is the minimization  
383 of the air jet indentation system for portable or endoscopic uses [50-52]. In such cases,  
384 the probe can be portable for flexible use in various body sites or small enough to be  
385 inserted in endoscopy for internal tissue detection.

386 A hypothesis of the current study was that the air jet indentation was comparable to  
387 the standard indentation with a rigid indenter and then the stiffness of specimen was  
388 simplified in an index coefficient of the force/deformation ratio. The high correlation of  
389 the stiffness coefficients between the air jet indentation and standard indentation really  
390 showed that these two tests were similar. The high correlation between the stiffness  
391 coefficient and the Young's modulus showed in a further step that the stiffness  
392 coefficient could be used as a quantitative measure of the specimen elasticity. Thus the  
393 developed OCT-based air jet indentation system can be further applied to a host of body  
394 tissues for clinical diagnoses, such as skin cancer, burn status, corneal condition, blood  
395 vessel stiffening and articular cartilage degeneration, where the change of tissue elasticity  
396 is obviously involved from clinical observations.

397 However, intrinsic mechanical properties such as the Young's modulus are more  
398 preferable for widespread applications because this will further enable the inter-lab or  
399 inter-hospital comparisons of respective studies. Therefore, further investigations are  
400 needed to extract the intrinsic mechanical properties from the air jet indentation test. This  
401 is thought to be complicated due to two main reasons: complicated mechanical behaviors  
402 of the soft tissues under rigid indentation, and the complicated interactions between the  
403 air jet and the soft tissues in air jet indentation. The first issue was addressed previously  
404 in a lot of studies [23,48,53-55]. In linear elasticity theory, the factors that affect the

405 extractions of the elastic modulus include the Poisson's ratio, indenter shape,  
406 force/indentation ratio and the initial thickness. When the theory is applied to real tissues  
407 *in vivo*, careful protocols should be designed to account for the extra effects from  
408 viscoelasticity, nonlinearity, non-homogeneity and anisotropy of the tissue properties. In  
409 this study, homogeneous and isotropic silicone phantoms were fabricated so as to  
410 simplify the mechanical behavior of the specimen. The stiffness coefficient or Young's  
411 modulus was obtained with the constraint of 3% of the deformation/thickness ratio or  
412 strain, which was thought to be a linear elasticity region for most soft tissues [49]. The  
413 viscosity was neglected in the study because it was not so obviously observed for the  
414 silicone phantoms fabricated in this study.

415 On the other hand, the interactions between the air jet and soft tissues are much less  
416 studied because the air jet indentation for the measurement of tissue elasticity was a novel  
417 approach in biomedical engineering field. The waterjetting, similar to the air jet, is a  
418 technique which has found widespread applications in a variety of industries [56].  
419 However, the previous analysis on waterjetting could not be directly applied to our  
420 studies because most of the industrial applications focus on material cutting and cleaning,  
421 where the water pressure is much higher than that used in the current study. The  
422 difference between the rigid indention and air jet indentation is that the tissue under the  
423 rigid indenter is uniformly compressed with a planar surface in the former case while this  
424 may not be the truth for the air jet one. It is expected that the deformation profile as well  
425 as the pressure distribution in the interaction surface keeps changing as the change of the  
426 air jet pressure. Finite element analysis, as used in previously indentation studies [57-60],  
427 may be incorporated in further studies for the analysis of the air jet indentation to

428 investigate the interactions between the air jet and tissues and the effects of the variations  
429 including the Poisson's ratio, the air jet radius, the distance between the bubbler tip and  
430 the tissue surface, and the tissue thickness.

## 431 **5. Conclusion**

432 A novel OCT-based air jet indentation system was developed in the current study.  
433 OCT can be used to detect tissue deformation as small as submicrons in a noncontact way.  
434 The high correlation of the stiffness measured by the current system with that obtained by  
435 the conventional and standard methods indicated that mechanical test with the OCT-  
436 based air jet indentation was feasible. The capacity of the system to detect the  
437 biomechanical changes in soft tissues had been demonstrated by phantom study and  
438 preliminary *in-vivo* test. Further improvements are required to include lateral scanning  
439 functions so as to map the tissue elasticity and to enhance the stability of OCT signal  
440 from skin surface for *in-vivo* applications where the motion artifacts cannot be avoided.  
441 The combination of the proposed air jet technique into the OCT elastography methods  
442 recently reported in the literature [18,20-21,61-62] may be able to provide noncontact  
443 OCT elasticity imaging for tissues. Testing on more tissues to demonstrate the potential  
444 of this system for widespread applications in biomedical engineering is under planning.

445

## 446 **ACKNOWLEDGEMENTS**

447 We would like to thank the helps from Mr. Chi-Fai Tin in the workshop of HTI  
448 department, Hong Kong Polytechnic University, for the set up of the system. This work  
449 was partially supported by Hong Kong Research Grants Council (PolyU5318/05E) and  
450 the Hong Kong Polytechnic University (J-BB69).



452 **REFERENCES**

- 453 1. Mridha M and Odman S 1986 Noninvasive method for the assessment of  
454 subcutaneous edema *Med. Biol. Eng. Comput.* **24** 393-398
- 455 2. Garra B S, Cespedes E I, Ophir J, Spratt S R, Zuurbier R A, Magnant C M and  
456 Pennanen M F 1997 Elastography of breast lesions: Initial clinical results *Radiology*  
457 **202** 79-86
- 458 3. McKnight A L, Kugel J L, Rossman P J, Manduca A, Hartmann L C and Ehman R  
459 L 2002 MR elastography of breast cancer: Preliminary results *Am. J. Roentgenol.*  
460 **178** 1411-1417
- 461 4. Davis A M, Dische S, Gerber L, Saunders M, Leung S F and O'Sullivan B 2003  
462 Measuring postirradiation subcutaneous soft-tissue fibrosis: State-of-the-art and  
463 future directions. *Semin. Radiat. Oncol.* **13** 203-213
- 464 5. Ophir J, Cespedes I, Ponnekanti H, Yazdi Y and Li X 1991 Elastography - A  
465 quantitative method for imaging the elasticity of biological tissues *Ultrasonic*  
466 *Imaging* **13** 111-134
- 467 6. Parker K J, Gao L, Lerner R M and Levinson S F 1996 Techniques for elastic  
468 imaging: A review *IEEE Eng. Med. Biol.* **15** 52-59
- 469 7. Zheng Y P and Mak A F T 1996 An ultrasound indentation system for  
470 biomechanical properties assessment of soft tissues in-vivo *IEEE Trans. Biomed.*  
471 *Eng.* **43** 912-918
- 472 8. Fatemi M and Greenleaf F J 1998 Ultrasound-stimulated vibro-acoustic  
473 spectrography *Science* **280** 82-85

- 474 9. Sarvazyan A P, Rudenko O V, Swanson S D, Fowlkes J B and Emelianov S Y 1998  
475 Shear wave elasticity imaging - A new ultrasonic technology of medical diagnostics  
476 *Ultrasound Med. Biol.* **24** 1419-1435
- 477 10. Diridollou S, Patat F, Gens F, Vaillant L, Black D, Lagarde J M, Gall Y and Berson  
478 M 2000 In vivo model of the mechanical properties of the human skin under suction  
479 *Skin Res. Tech.* **6** 214-221
- 480 11. Nightingale K R, Palmeri M L, Nightingale R W and Trahey G E 2001 On the  
481 feasibility of remote palpation using acoustic radiation force *J. Acoust. Soc. Am.* **110**  
482 625-634
- 483 12. Sandrin L, Tanter M, Gennisson J L, Catheline S and Fink M 2002 Shear elasticity  
484 probe for soft tissues with 1-D transient elastography *IEEE Trans. Ultrason.*  
485 *Ferroelec. Freq. Contr.* **49** 436-446
- 486 13. Zheng Y P, Mak A F T, Lau K P and Qin L 2002 An ultrasonic measurement for in  
487 vitro depth-dependent equilibrium strains of articular cartilage in compression *Phys.*  
488 *Med. Biol.* **47** 3165-3180
- 489 14. Konofagou E E and Hynynen K 2003 Localized harmonic motion imaging: Theory,  
490 simulations and experiments *Ultrasound Med. Biol.* **29** 1405-1413
- 491 15. Zheng YP, Bridal SL, Shi J, Saied A, Lu MH, Jaffre B, Mak AFT and Laugier P  
492 2004 High resolution ultrasound elastomicroscopy imaging of soft tissues: System  
493 development and feasibility *Phys. Med. Biol.* **49** 3925-3938
- 494 16. Muthupillai R, Lomas D J, Rossman P J, Greenleaf J F, Manduca A and Ehman R L  
495 1995 Magnetic resonance elastography by direction visualization of propagating  
496 acoustic strain waves *Science* **269** 1854-1857

- 497 17. Asserin J, Agache P and Humbert P 1995 Checking the mechanical performances of  
498 a skin suction meter - The Cutometer *J. Invest. Dermatol.* **104** 165-165
- 499 18. Schmitt J M 1998 OCT elastography: imaging microscopic deformation and strain  
500 of tissue *Opt. Express* **3** 199-211
- 501 19. Duda G N, Kleemann R U, Bluecher U and Weiler A 2004 A new device to detect  
502 early cartilage degeneration *Am. J. Sports. Med.* **32** 693-698
- 503 20. Khalil A S, Chan R C, Chau A H, Bouma B E and Mofrad M R K 2005 Tissue  
504 elasticity estimation with optical coherence elastography: Toward mechanical  
505 characterization of in vivo soft tissue *Ann. Biomed. Eng.* **33** 1631-1639
- 506 21. Kirkpatrick S J, Wang R K, Duncan D D, Kulesz-Martin M and Lee K 2006  
507 Imaging the mechanical stiffness of skin lesions by in vivo acousto-optical  
508 elastography *Opt. Express* **14** 9770-9779
- 509 22. Mazza E, Nava A, Halmloser D, Jochum W and Bajka M 2007 The mechanical  
510 response of human liver and its relation to histology: An in vivo study *Med. Image  
511 Anal.* **11** 663-672
- 512 23. Hayes W C, Herrmann G, Mockros L F and Keer L M 1972 A mathematical  
513 analysis for indentation tests of articular cartilage *J. Biomech.* **5** 541-551
- 514 24. Lyyra T, Jurvelin J, Pitkanen P, Vaatainen U and Kiviranta I 1995 Indentation  
515 instrument for the measurement of cartilage stiffness under arthroscopic control *Med.  
516 Eng. Phys.* **17** 395-399
- 517 25. Stahl R, Blumenkrantz G, Carballido-Gamio J, Zhao S, Munoz T, Le Graverand-  
518 Gastineau M P H, Li X, Majumdar S and Link T M 2007 MRI-derived T2 relaxation

- 519 times and cartilage morphometry of the tibio-femoral joint in subjects with and  
520 without osteoarthritis during a 1-year follow-up *Osteoarthr. Cartilage* **15** 1225-1234
- 521 26. Appleyard R C, Burkhardt D, Ghosh P, Read R, Cake M, Swain M V and Murrell G  
522 A C 2003 Topographical analysis of the structural, biochemical and dynamic  
523 biomechanical properties of cartilage in an ovine model of osteoarthritis *Osteoarthr.*  
524 *Cartilage* **11** 65-77
- 525 27. Zheng Y P and Mak A F T 1999 Effective elastic properties for lower limb soft  
526 tissues from manual indentation experiment *IEEE Trans. Rehabil. Eng.* **7** 257-267
- 527 28. Zheng Y P, Mak A F T, and Lue B K 1999 Objective assessment of limb tissue  
528 elasticity: development of a manual indentation procedure *J. Rehabil. Res. Dev.* **36**  
529 71-85
- 530 29. Zheng Y P, Choi Y K C, Wong K, Chan S and Mak A F T 2000 Biomechanical  
531 assessment of plantar foot tissue in diabetic patients using an ultrasound indentation  
532 system *Ultrasound Med. Biol.* **26** 451-456
- 533 30. Leung S F, Zheng Y P, Choi C Y K, Mak S S S, Chiu S K W, Zee B and Mak A F T  
534 2002 Quantitative measurement of post-irradiation neck fibrosis based on the young  
535 modulus - Description of a new method and clinical results *Cancer* **95** 656-662
- 536 31. Huang Y P, Zheng Y P and Leung S F 2005 Quasilinear viscoelastic parameters of  
537 neck tissues with fibrosis induced by radiotherapy *Clin. Biomech.* **20** 145-154
- 538 32. Lau J, Li W P C and Zheng Y P 2005 Application of tissue ultrasound palpation  
539 system (TUPS) in objective scar evaluation *Burns* **31** 445-452
- 540 33. Li-Tsang C W P, Lau J C M and Chan C C H 2005 Prevalence of hypertrophic scar  
541 formation and its characteristics among the Chinese population *Burns* **31** 610-616

- 542 34. Zheng Y P, Li Z M, Choi A P C, Lu M H, Chen X and Huang Q H 2006 Ultrasound  
543 palpation sensor for tissue thickness and elasticity measurement - Assessment of  
544 transverse carpal ligament *Ultrasonics* **44** e313-e317
- 545 35. Suh J K F, Youn I and Fu F H 2001 An in situ calibration of an ultrasound  
546 transducer: A potential application for an ultrasonic indentation test of articular  
547 cartilage *J. Biomech.* **34** 1347-1353
- 548 36. Laasanen M S, Saarakkala S, Toyras J, Hirvonen J, Rieppo J, Korhonen R K and  
549 Jurvelin J S 2003 Ultrasound indentation of bovine knee articular cartilage in situ. *J.*  
550 *Biomech.* **36** 1259-1267
- 551 37. Lu M H, Zheng Y P and Huang Q H 2005 A novel noncontact ultrasound  
552 indentation system for measurement of tissue material properties using water jet  
553 compression *Ultrasound Med. Biol.* **31** 817-826
- 554 38. Lu M H, Zheng Y P and Huang Q H 2007 A novel method to obtain modulus image  
555 of soft tissues using ultrasound water jet indentation: A phantom study *IEEE Trans.*  
556 *Biomed. Eng.* **54** 114-121
- 557 39. Lu MH, Zheng YP, Huang QH, Ling HY, Wang Q, Bridal SL, Qin L and Mak AFT  
558 2007 Noncontact evaluation of articular cartilage degeneration using a novel  
559 ultrasound water jet indentation system *Annals of Biomedical Engineering* Under  
560 review
- 561 40. Lu MH, Zheng YP, Lu HB, Huang QH and Qin L 2008. A noncontact ultrasound  
562 method for evaluation of bone-tendon junction healing *Ultrasound in Medicine and*  
563 *Biology* Under review

- 564 41. Cote G L, Lec R M and Pishko M V 2003 Emerging biomedical sensing  
565 technologies and their applications *IEEE Sens. J.* **3** 251-266
- 566 42. Huang D, Swanson E A, Lin C P, Schuman J S, Stinson W G, Chang W, Hee M R,  
567 Flotte T, Gregory K, Puliafito C A and Fujimoto J G 1991 Optical coherence  
568 tomography *Science* **254** 1178-1181
- 569 43. Drexler W 2004 Ultrahigh-resolution optical coherence tomography *J. Biomed. Opt.*  
570 **9** 47-74
- 571 44. Leitgeb R A, Drexler W, Unterhuber A, Hermann B, Bajraszewski T, Le T, Stingl A  
572 and Fercher A F 2004 Ultrahigh resolution Fourier domain optical coherence  
573 tomography *Opt. Express* **12** 2156-2165
- 574 45. Chen Z P, Zhao Y H, Srivivas S M, Nelson J S, Prakash N and Frostig R D 1999  
575 Optical Doppler tomography *IEEE J. Select. Topics Quantum Electro.* **5** 1134-1142.
- 576 46. Bohnke M, Masters B R, Walti R, Ballif J J, Chavanne P, Gianotti R and Salathe R  
577 P 1999 Precision and reproducibility of measurements of human corneal thickness  
578 with rapid optical low-coherence reflectometry (OLCR) *J. Biomed. Opt.* **4** 152-156
- 579 47. Tomlins P H and Wang R K 2005 Theory, developments and applications of optical  
580 coherence tomography *J. Phys. D Appl. Phys.* **38** 2519-2535
- 581 48. Waters N E 1965 Indentation of thin rubber sheets by cylindrical indentors *Br. J.*  
582 *Appl. Phys.* **16** 1387-1392
- 583 49. Nitta N and Shiina T 2002 A visualization of nonlinear elasticity property of tissues  
584 by ultrasound *Electron. Comm. Jpn.* **85** 9-18
- 585 50. Sergeev A, Gelikonov V, Gelikonov G, Feldchtein F, Kuranov R, Gladkova N,  
586 Shakhova N, Snopova L, Shakhov A, Kuznetzova I, Denisenko A, Pochinko V,

- 587 Chumakov Y and Streltzova O 1997 In vivo endoscopic OCT imaging of  
588 precancerand cancer states of human mucosa *Opt. Express* **1** 432-440
- 589 51. Tearney G J, Brezinski M E, Bouma B E, Boppart S A, Pitris C, Southern J F and  
590 Fujimoto J G 1997 In vivo endoscopic optical biopsy with optical coherence  
591 tomography *Science* **276** 2037-2039
- 592 52. Boppart S A, Bouma B E, Pitris C, Tearney G J, Fujimoto J G and Brezinski M E  
593 1997 Forward-imaging instruments for optical coherence tomography *Opt. Lett.* **22**  
594 1618-1620
- 595 53. Mak A F, Lai W M and Mow V C 1987 Biphasic indentation of articular-cartilage. 1.  
596 Theoretical analysis *J. Biomech.* **20** 703-714
- 597 54. Mow V C, Gibbs M C, Lai W M, Zhu W B and Athanasiou K A 1989 Biphasic  
598 indentation of articular-cartilage. 2. A numerical algorithm and an experimental  
599 study *J. Biomech.* **22** 853-861
- 600 55. Yu W P and Blanchard J P 1996 An elastic-plastic indentation model and its  
601 solutions *J. Mater. Res.* **11** 2358-2367
- 602 56. Summers D A 1995 *Waterjetting Technology*: Taylor & Francis
- 603 57. Suh J K and Spilker R L 1994 Indentation analysis of biphasic articular cartilage -  
604 Nonlinear phenomena under finite deformation *J. Biomech. Eng. - T. ASME* **116** 1-9
- 605 58. Zhang M, Zheng Y P and Mak A F T 1997 Estimating the effective Young's  
606 modulus of soft tissues from indentation tests - Nonlinear finite element analysis of  
607 effects of friction and large deformation *Med. Eng. Phys.* **19** 512-517

- 608 59. Tonuk E and Silver-Thorn M B 2003 Nonlinear elastic material property estimation  
609 of lower extremity residual limb tissues *IEEE Trans. Neural Syst. Rehab. Eng.* **11**  
610 43-53
- 611 60. Lu M H and Zheng Y P 2004 Indentation test of soft tissues with curved substrates:  
612 A finite element study *Med. Biol. Eng. Comput.* **42** 535-540
- 613 61. Kirkpatrick S J, Wang R K and Duncan DD 2006 OCT-based elastography for large  
614 and small deformations *Opt. Express* **14** 11585-11597
- 615 62. Wang R K K, Ma Z H and Kirkpatrick S J 2006 Tissue Doppler optical coherence  
616 elastography for real time strain rate and strain mapping of soft tissue *App. Phys.*  
617 *Lett.* **89** 144103
- 618

619 **Figure captions:**

620 Figure 1. (a) Schematic of the OCT-based air jet indentation system; (b) A picture of the  
621 real system.

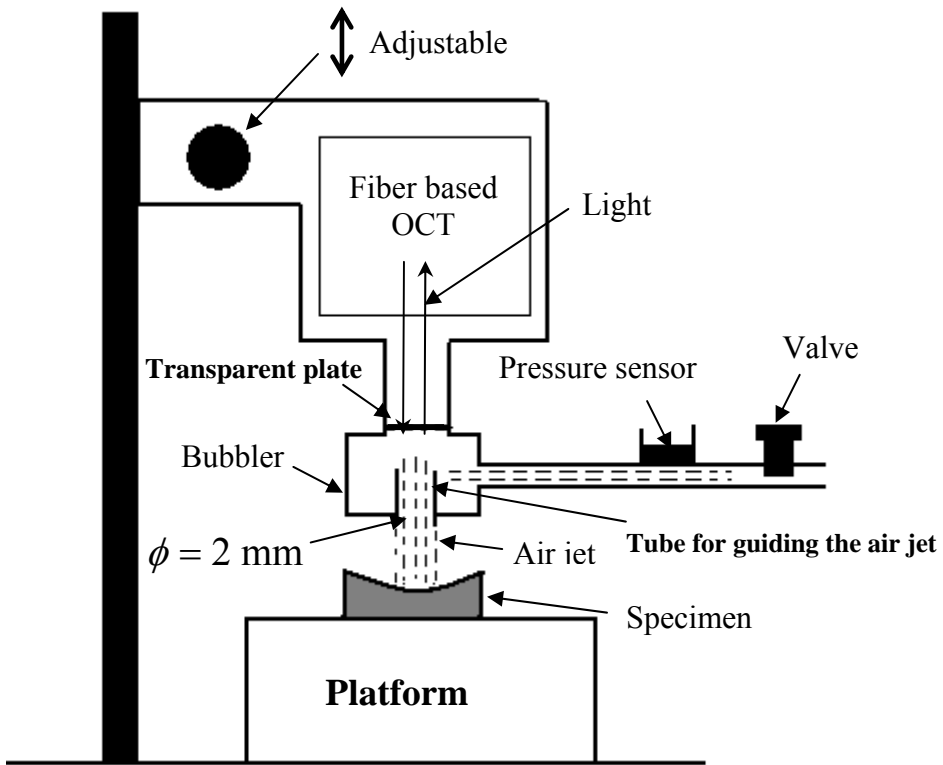
622 Figure 2. The diagram of the air jet indentation and data collection modules of the air jet  
623 indentation system.

624 Figure 3. The custom-designed software interface for the real-time data acquisition and  
625 post-acquisition off-line processing such as the displacement extraction. The left of the  
626 window shows the control panels for data acquisition and post-acquisition processing.  
627 The measured pressure and extracted deformation as well as the OCT signal are  
628 displayed on the right.

629 Figure 4. *In vivo* experiment on the hand soft tissues. (a) Soft tissues indented without  
630 muscle contraction; (b) Soft tissues with muscle contraction.

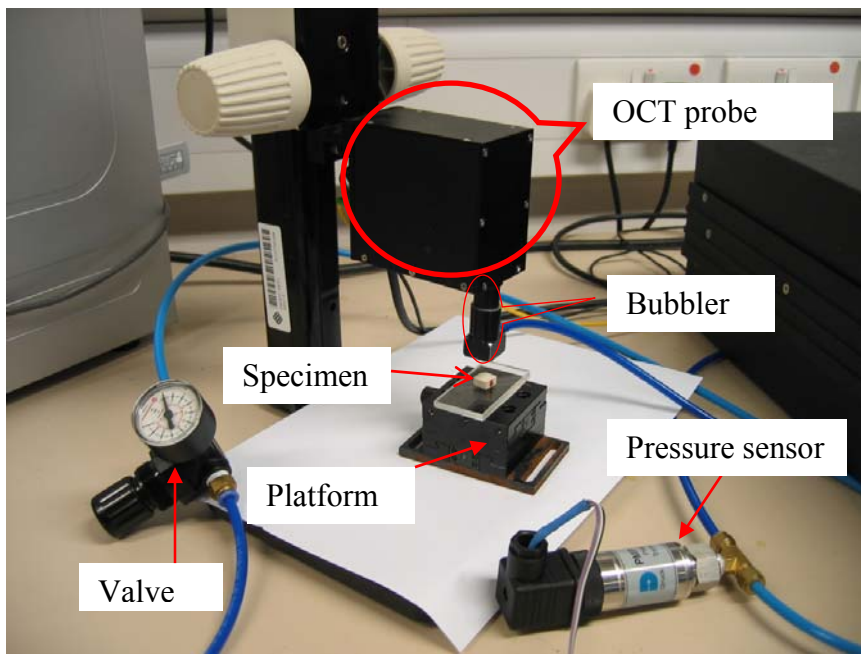
631 Figure 5. Representative indentation curves on one phantom. (a) Force-deformation  
632 curves obtained during loading and unloading cycles; (b) The relationship between the  
633 force and deformation of the phantom.

634 Figure 6. (a) Correlation of stiffness coefficients measured by the air jet and standard  
635 indentation test; (b) correlation of stiffness coefficient measured by the air jet indentation  
636 test and the Young's modulus measured by standard compression test.



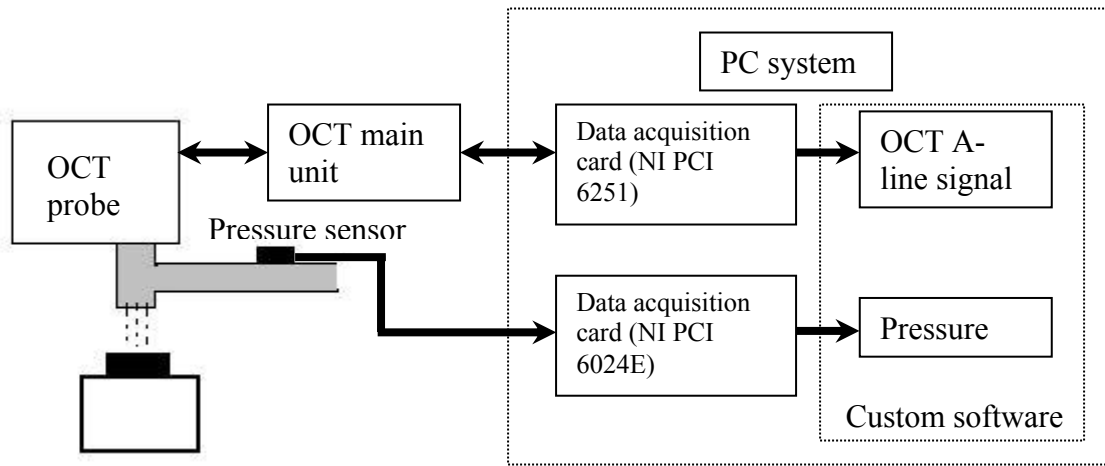
637

638 Fig. 1 (a)



639

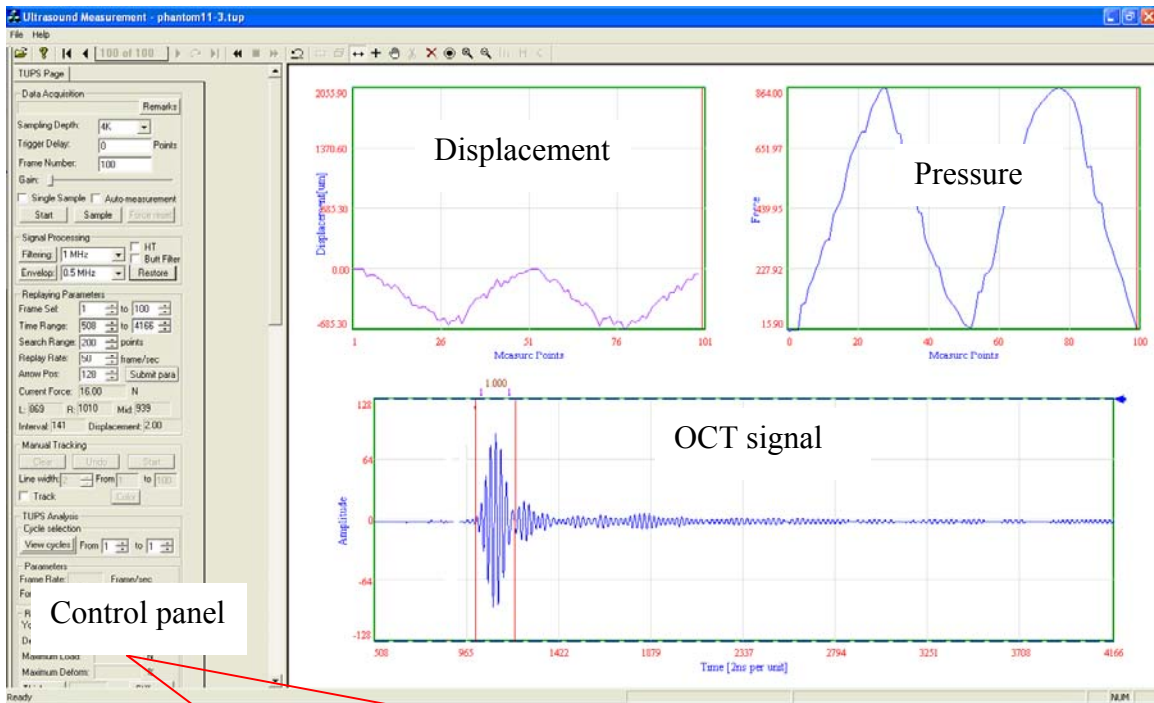
640 Fig. 1 (b)



641

642

643 Fig. 2



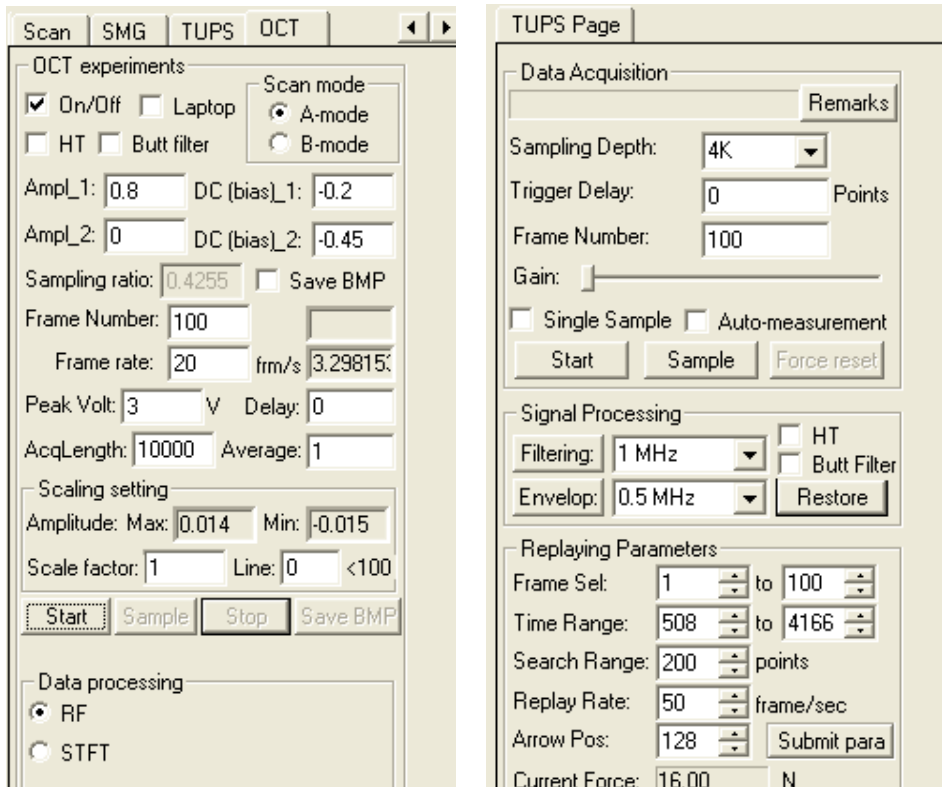
644

645

Control panel

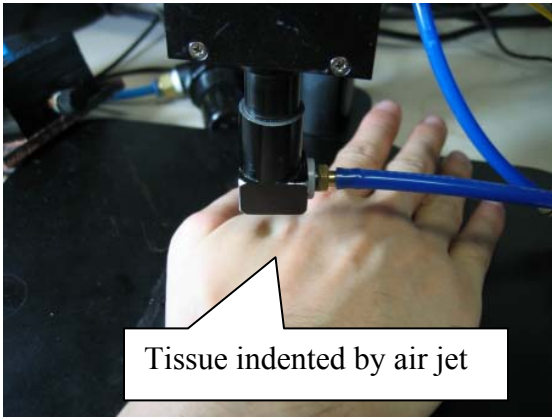
Used for acquisition

Used for post-acquisition processing



646

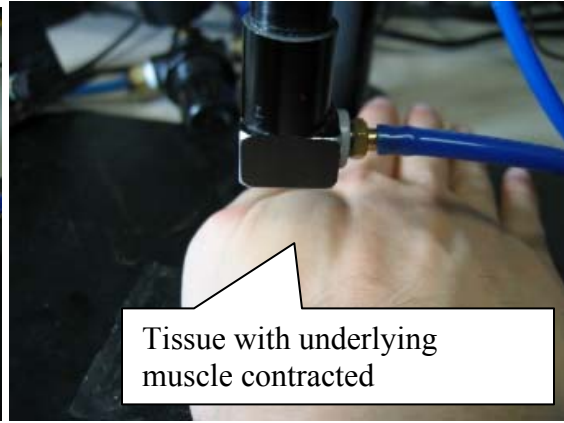
647 Fig. 3



648

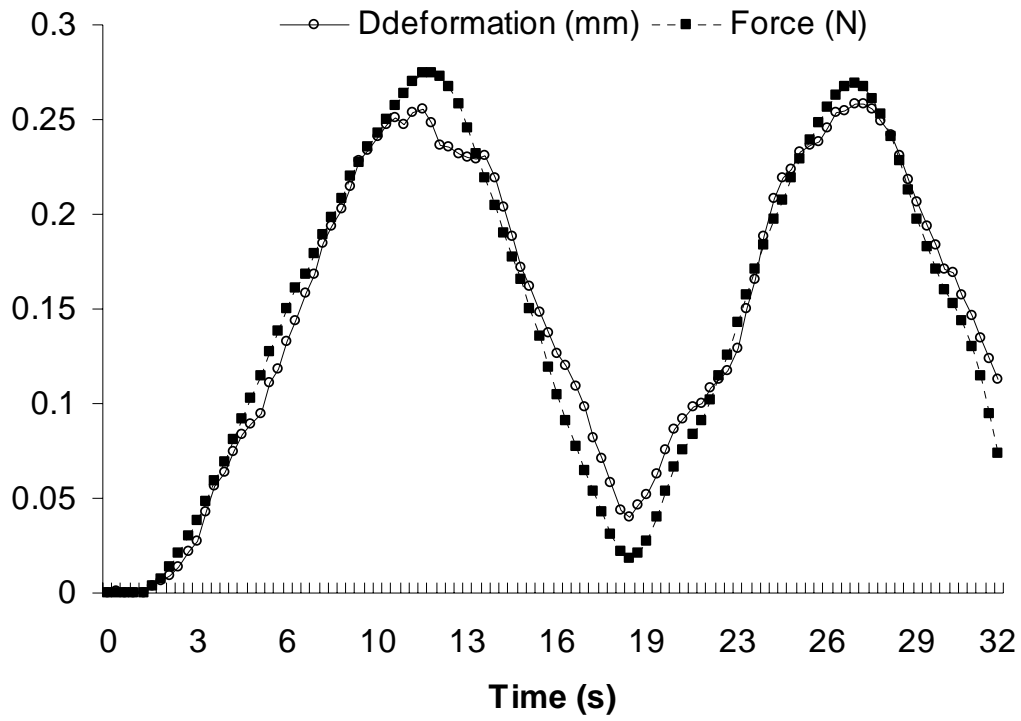
649

(a)



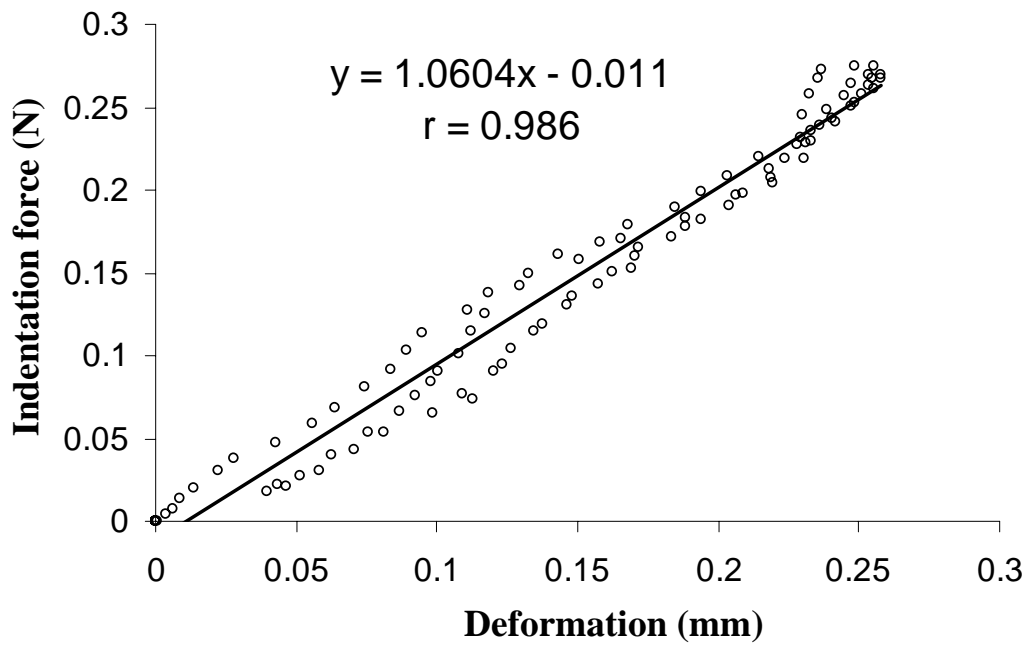
(b)

650 Fig. 4 (a) & (b)



651

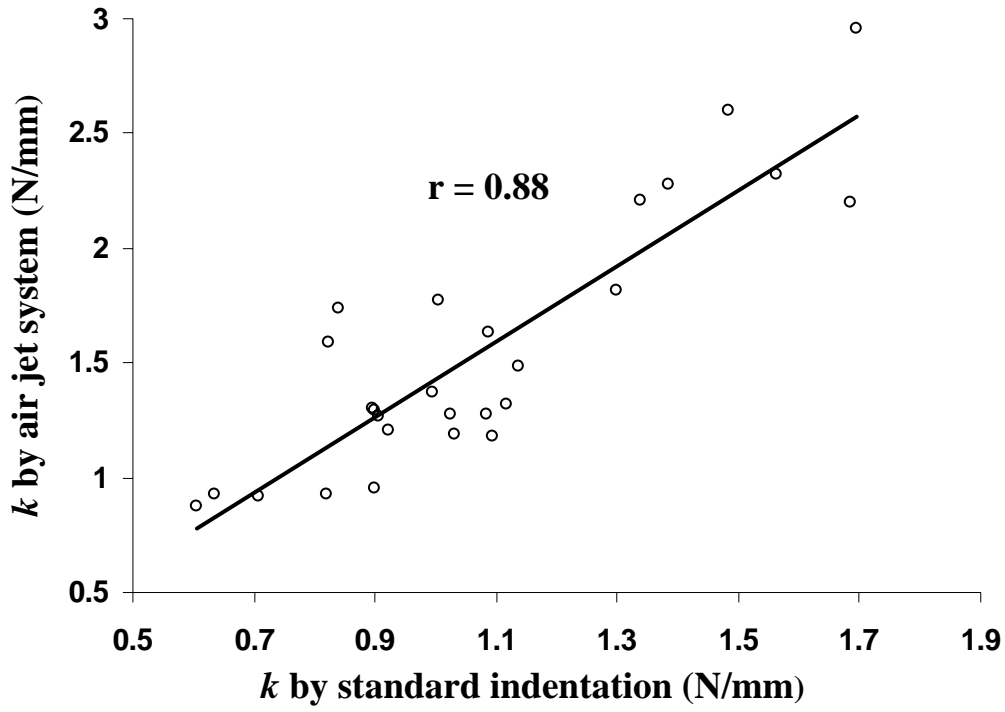
652 Fig. 5 (a)



653

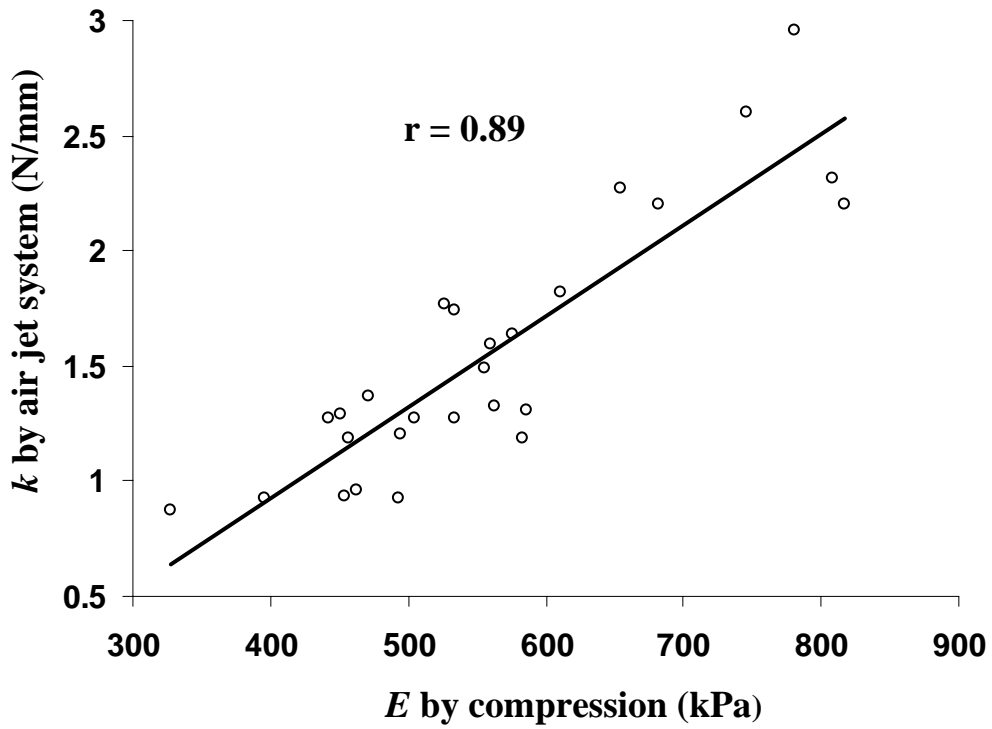
654 Fig. 5 (b)

655



656

657 Fig. 6 (a)



658

659 Fig. 6 (b)